*Determination of Inventories and Power Distributions for the NBSR**
Presented at the TRTR/IGORR Joint Meeting
Gaithersburg, Md.
September 12-16, 2005

A.L. Hanson and D.J. Diamond
Energy Sciences and Technology Department
Brookhaven National Laboratory

*This work was performed under the auspices of the U.S. Department of Energy,
Contract No. DE-AC02-98CH10886

Determination of Inventories and Power Distributions for the NBSR
Presented at the TRTR/IGORR Joint Meeting
Gaithersburg, Md.
September 12-16, 2005

A.L. Hanson and D.J. Diamond
Energy Sciences and Technology Department
Brookhaven National Laboratory

Abstract

This memo presents the details of the methodology for developing fuel inventories for the NBSR along with power distributions predicted with this set of inventories. Several improvements have been made to the MCNP model of the NBSR since a set of calculations was performed in 2002 in support of the NBSR relicensing and SAR update. One of the most significant changes in the model was to divide the fuel elements into upper and lower halves so the effects of uneven burn between the two halves (due to the shim arms) can be determined. The present set of power distributions are provided for comparison with the previous safety analyses.

The NBSR Fuel Management Scheme

Figure 1 shows the thirty positions in the NBSR where fuel elements are located. There are seven numbered rows and thirteen lettered columns. The position denoted with <RR> is the position of the regulating rod and the six positions denoted with <> are the 3-½ in in-core irradiation thimbles. These thimbles are aluminum tubes assumed to be filled with D_2O only. The four 2-½ in in-core irradiation thimbles located in positions D4, G3, G5, and J4 are not included in this figure, but are included in the neutronics model.

The fuel management scheme for the NBSR is shown in Figure 2. Each fuel position is denoted with two numbers and one letter. The letters are either E or W for the east or west side of the core noting that a fuel element always stays in the east side or in the west side of the core. Since there are thirty fuel elements, 16 stay in the core for eight cycles and 14 stay in the core for seven cycles. The first number denotes how many cycles the element will be in the core (either 8 or 7) and the second number denotes the cycle in which the fuel element resides. Therefore at the beginning of a cycle, the 8-1 and 7-1 fuel elements are fresh, unirradiated fuel elements, 8-8 and 7-7 are in their final cycles and will be removed after the cycle is over. After a cycle is finished the 8-8 and 7-7 fuel elements are removed and the 8-7 elements are moved into the 8-8 positions, the 7-6 elements are moved into the 7-7 positions. Likewise the 8-6 and 7-5 fuel elements are moved into the 8-7 and 7-6 positions, respectively. This keeps occurring until the 8-1 and 7-1 fuel elements are moved into the 8-2 and 7-2 positions and new, unirradiated fuel is placed in the 8-1 and 7-1 positions. It should be recognized that the 7-1 through 7-7 and 8-1 through 8-8 denotations are the representations for the upper half of the fuel elements. The lower halves of the fuel elements are denoted with 5-1 through 5-7, which

correspond to the 7-1 through 7-7 half fuel elements, and 6-1 through 6-8 which correspond to the 8-1 through 8-8 half fuel elements. By dividing the fuel in this manner there are 30 different materials that are determined for the NBSR fuel inventory. Inherent to this analysis was to invoke East-West symmetry, that is, it is assumed that the inventory in the elements with the same numbering scheme but a different E or W designation have the identical inventory.

Determination of Inventory with MONTEBURNS

The NBSR has 30 fuel elements divided into upper and lower halves. There is a 0.177 m (7 in) gap between the two halves. In order to define inventories and determine the burn-up one explicitly defines a material for each different fueled region that will be analyzed. If we were to model each half every fuel element, there would be a total of 60 materials. However there is a fundamental limit of 49 materials that can be tracked with the code system that was used, MOTEBURNS [1]. This limitation is due to the number of tallies (tallies in MCNP are the commands that determine what outputs the code is to generate) that are available in MCNP [2], which are discussed below. Therefore there was a choice to be made; either assume East-West symmetry or Upper-Lower symmetry. Because the shim arms are partially inserted in the Upper core and not in the Lower core, the choice was to assume East-West symmetry. Therefore the material in the 7-3E half element has the identical inventory as the 7-3W half element, etc.

Inventories for the 30 different fuel materials were generated with the MONTEBURNS code system. MONTEBURNS is a computer code system that invokes the neutronics code MCNP [3] and the burn-up code ORIGEN2 [4]. Because of the availability of a new version of MONTEBURNS, compatible with MCNP5, the previous MCNP model for the NBSR [as described in 5] has been modified and converted to use the cross section files supplied with MCNP5.

At the start of the MONTEBURNS analyses, the initial inventory in each fuel region was the one originally determined [5] without accounting for differences between the fuel above and below the mid-plane gap. The calculations assume an initial fuel inventory and follow ten 38-day cycles to eliminate errors in the initial estimate. After about four cycles, the ^{235}U concentrations in the fuel elements came close to the final concentrations. There was only minimal fluctuation around the final values, the largest being 1.8% with most in the 0.3% range. When using the MONTEBURNS code system, it is not possible to change the position of the shim arms as one progresses through a fuel cycle. Therefore for these calculations the shim arms were placed at a mid-cycle position of 12 degrees below vertical. In addition the regulating rod was positioned at 50% withdrawn.

MONTEBURNS functions by inserting tallies in the MCNP input deck that instructs MCNP to calculate the neutron spectra and one-group neutron cross sections for each individual fuel material. With this, each user-defined material has a set of neutron cross-sections for the time step represented by that inventory. The cross sections generated by MCNP are then used in the ORIGEN2 burn-up calculations, so the cross sections used by ORIGEN2 are appropriate for each local neutron flux. After ORIGEN2 has been used to determine the local (the individual material) inventory and local burn-up for a particular time step, MONTEBURNS rewrites the material inventories in the MCNP

input deck. MCNP is then rerun with the new inventory. It now calculates new local neutron fluxes and new one-group cross sections. ORIGEN2 is then rerun, and so forth. One feature of MONTEBURNS is that one can remove and insert fuel along with redistributing the remaining fuel between the fuel cycles.

A problem now arises. Most of the radioactive fission products that ORIGEN2 can calculate are not supported by the cross section files supplied with MCNP. The result is that the isotopes determined by ORIGEN2 that should be in the inventory and are not compatible with the MCNP cross section libraries are "discarded", that is removed from the inventory. This results in unaccounted mass. MONTEBURNS must now deal with this missing mass since MCNP normalizes all mass (or atomic) fractions to unity. If mass is artificially missing, after MCNP normalizes the materials to unity, the mass of all isotopes in the material will be increased, so there would be too much fissionable material. MONTEBURNS deals with this issue by determining the mass of material that it is not counting and reducing the density of the materials accordingly. This way it maintains the correct mass of the isotopes that it is following. For the NBSR the amount of material that ORIGEN2 calculates to be in the inventory that is not supported by the MCNP libraries is, on average, 1.2% of the total mass in the fuel element per cycle, so the 6-8 and 8-8 fuel elements are "missing" almost 10% of their mass. This is demonstrated in Figure 3, a plot of the change in density as calculated by MONTEBURNS as a function of completed cycle for the four different series (5*, 6*, 7*, 8*). The statement "as a function of completed cycle" means the density plotted is the densities for the end-of-cycle inventories for the *1 through *8 fuel elements.

There are cross section files for some of the radioisotopes that are not supported by MCNP. These files are available from MIT and the U. Texas. However, if one includes as many actual fission products as possible, the result is a set of inventories so large that the speed of the computation becomes prohibitively slow. With the present inventories, the end-of-cycle equilibrium core has more than 60 isotopes in some of the materials. The total core inventory contains more than 1650 entries over the 30 different materials.

MONTEBURNS maintains a set of files for all of the MCNP calculations. The inventories that were generated for this work were extracted from the last file, i.e. the last time step of the final cycle followed. One could use these inventories as long as one also used the modified densities. However, these densities, some as much as 9-10% low, would not be appropriate for power distribution calculations. It would also mean that each material will have a different density and that each material's density changes on the average 1.2% during a fuel cycle.

The creation of a set of inventories from the MONTEBURNS calculations therefore requires some processing of the data. The starting point is the final MCNP input file written. This represents the end-of-cycle (EOC) equilibrium core. In order to use the correct density, mass fractions of all of the isotopes were adjusted by the ratio of the modified density to the actual density with the exception of oxygen and aluminum. Their atomic fractions were set to the values in the fresh, unirradiated fuel. This is a reasonable assumption since the cross sections for thermal neutron absorption by these elements are less than a barn: for oxygen it is 0.27 b and for aluminum it is 0.23 b. Examining the output files of MONTEBURNS indicated that allowing transmutation of

these elements would result in less than a 0.5% change in their concentrations over 8 cycles.

Adjusting the mass fractions by the ratio of the densities maintains the calculated masses of the isotopes being followed. Now the sum of all of the mass fractions is less than unity. In order to deal with the "missing mass" while maintaining the proper density it was assumed that "representative" fission products can be included as part of the inventory, their mass fraction being the balance that brings the total back to unity. In the previous analyses [5, 6, 7], the missing mass was distributed evenly between natural zirconium, natural tin, and ^{138}Ba. These have thermal neutron cross sections of 0.18b, 0.63b and 0.38b, respectively.

However, because of the analysis of the burn-up of the cadmium shim arms, it became apparent that these surrogate isotopes did not provide enough cross section for adequate absorption of neutrons by the fission products in the fuel. The absorption averaged over all fission products is ~50b/fission or ~25b per fission product [8]. Some of this absorption is accounted for in the high absorption isotopes that have cross section libraries supplied with MCNP libraries: ^{135}Xe, ^{147}Nd, ^{149}Pm, and ^{105}Rh. The issue became apparent when the calculated critical positions of the shim arms were considerably different from the measured values in later stages of the reactor cycle. As an example after 28.5 days of operation (3/4 through a cycle) the calculated critical angle was -10° from vertical as opposed to the actual -5°. The issue was solved by replacing the natural zirconium with ^{133}Cs which has a thermal neutron absorption cross section of 29.9b. With this change, the calculated shim arm positions are in good agreement with the measured positions for six different core inventories. The critical angles for the six different inventories along with the calculated values of k_{eff}, as calculated by MCNP are shown in Table 1. This also means that during the MONTEBURNS calculations, there is an inappropriate amount of neutron absorption by the fission products.

At this point we now have the inventories for the EOC core. In order to determine the inventories for the Startup (SU) core we note that since all fuel elements are shifted by 1 (8-1 in the EOC core becomes an 8-2 in the next cycle). Therefore all isotopes are shifted to the next material, removing the old 5-7, 6-8, 7-7, and 8-8 inventories, and inserting the inventories for the fresh, unirradiated fuel in 5-1, 6-1, 7-1, and 8-1 materials. Since this refueling takes 11 days to complete, the shorter lived isotopes are allowed to decay to their daughter products. This is accomplished by adding the mass fraction of the parent isotope to the mass fraction of the daughter isotope and removing the parent isotope. The four isotopes removed this way are: ^{105}Rh ($t_{½}$=35.5 hr, σ_a=33000b), ^{135}Xe ($t_{½}$=9.16 hr, σ_a=2700000b), ^{149}Pm ($t_{½}$=9.16 hr, σ_a=1400b), and one half of ^{147}Nd ($t_{½}$=11.6 hr, σ_a=400b).

The one day equilibrium core was determined by running MONTEBURNS with the SU core for one day. The inventories for ¼, mid-, and ¾ cycles were determined from MONTEBURNS calculations starting with the one day equilibrium core. Each of these inventories needed to have their inventories adjusted as described for the EOC inventory.

Uranium Consumption.

One of the important parameters is the rate at which ^{235}U is burned during a cycle in each fuel element. Figure 4 shows the amount of ^{235}U burned in each fuel element during each cycle as was reported in the reference document [5]. For that work the fuel material was homogenized between the upper and lower portions of the fuel element, and is also the same for each element with an east or west designation (i.e. 7-4E has the same composition as 7-4W). Figure 5 shows the total amount of ^{235}U burned in each fuel element using the present model which models the top and bottom portions separately. Figure 6 shows the differences between the two analyses in percent. Overall there was an average of 5% difference between the two analyses.

In considering differences between the calculations presented in the [5] and the present effort, one should note that not only were there differences in the model of the reactor, but different versions of each code were used. In Reference 6 the codes used were MONTEBURNS Version 1.0, 1999 [9], MCNP4B [10], and ORIGEN2.1 [11], August 1991. For the present analysis the codes used were MONTEBURNS [1] Version 2, 2002, MCNP5 [3] and ORIGEN2.2 [4], June 2002. With MCNP4B the ENDFB-VI.0 (.60c) cross-section files were used wherever possible. With MCNP5 the ENDFB-VI.5 (.65c or .66c) cross-section files were used wherever possible. The earlier work was performed on a SUN2 system and the present analysis was performed on a PC. Since the speed of the PC is six times faster than the SUN2, better statistics for the neutronics analyses were possible. In the original model, the gap in the fuel element was modeled as a homogenized mix of aluminum and D_2O. The present model has the aluminum fuel element box filled with D_2O. The model of the shim arms has also been improved. With this, it is not surprising that there are significant differences between the original inventories and those generated for this work.

Figures 7 and 8 show the grams of ^{235}U burned during each cycle in each half of a fuel element; Figure 7 for the upper core and Figure 8 for the lower core. Figure 9 shows the percentage difference between the two half cores. As one considers differences in the amount of ^{235}U burned during each cycle between the upper and lower parts of the core, one should note that the four shim arms travel between rows 2 and 3, rows 3 and 4, rows 4 and 5, and rows 5 and 6. There are no shims traveling between rows 1 and 2 and between rows 6 and 7. One might expect a slight increase in the consumption in upper vs. lower half of the 7-2 fuel element since the lower half of the fuel element burned 3-4 grams more of ^{235}U in the lower half of the fuel element than in the upper half while the fuel element was residing in the 7-1 position. The calculations show that the 8-5 fuel element should have 3 grams more ^{235}U in the upper half than in the lower half. However it is situated next to the regulating rod, which was set at 50% withdrawal, so the upper half of this fuel element is more influenced by the regulating rod than the lower half and fuel consumption is suppressed.

Power Distributions

One major concern with the comparing the present set of inventories to the inventories developed for [5] is whether the results for the safety analyses in [5] are significantly affected. Figures 10 and 13 show the power distributions determined for [5] for the SU and EOC cores. For the SU core, the hottest fuel element F1 had a power 1.15 times the average. For the EOC core the A4 and M4 fuel elements had powers 1.10 times

the average. Because the MCNP model in Reference [5] did not distinguish between the upper and lower halves of the core, a series of calculations were performed that determined the difference between the power distributions in the two halves, which was referred to as the axial power factor. The axial power factor was calculated by selecting eight fuel elements (more than eight exceeded limitations of MCNP) and dividing them into 16 equally spaced regions (8 in the upper core and 8 in the lower core). Each region was ~3.5 cm long. The eight fuel elements chosen due are listed in Table 2. Of these, the H-1 fuel element the highest axial power peaking and was used for the safety analysis. From those axial power distributions, one can extract the relative power in the lower halves of the fuel elements, which are included in Table 2, column 3. Column 4 shows the values from the present analysis. Table 2 demonstrates that the present analysis shows consistently lower power factors than was used in Reference [5]. This is not surprising since the analysis in Reference [5] did not include differences in the ^{235}U content between the upper and lower cores; that is the fuel was forced to be homogenized over each fuel element. This meant the amount of ^{235}U in the lower half of the core was larger in the analysis for Reference [5] than it is in the present analysis. Therefore one can conclude that the conservative assumptions made for the safety analysis in Reference [5] are not negated by the present effort, but should be considered even more conservative than initially thought.

A comparison of the power distributions for the SU core between the two sets of analysis are shown in Figures 11 and 12. Figure 11 is the power distribution averaged over the upper and lower cores and Figure 12 shows the percent difference between the two analyses. For the present analysis, the hottest fuel element is still in the H-1 position, but the relative power factor is slightly lower than the previous analysis. Figures 14 and 15 show the results for the EOC cores.

Figures 16 and 17 show the power distributions for the upper and lower portions of the SU core and Figure 18 show the percent difference between them. The largest increases from the upper core to the lower core are the 7-1 fuel elements (the A4 and M4 positions), where the difference is a factor of two. The power distributions in these figures show that there is not true east-west symmetry for the fuel even though the fuel burn-up assumed east-west symmetry.

Figures 19 and 20 show the power distributions for the upper and lower portions of the EOC core and Figure 21 show the percent difference between them. These figures demonstrate that the power is shifted from the lower section of the core to the upper section of the core as the core progresses from the SU to the EOC state. However the difference in the power distribution between the two sections is smaller for the EOC core than for the SU core. This difference should be due to more ^{235}U in the upper core than the lower core. Figure 22 shows the power increase in the upper core as the core progresses from the SU to the EOC conditions and Figure 23 shows how the power is decreased in the lower core when progressing from the SU to the EOC core.

Acknowledgments

The work presented here was performed under the auspices of the National Institute of Standards and Technology (NIST) and was funded by the NIST Center for Neutron Research. The work was monitored at NIST by Dr. Seymour Weiss, whose support of this work was greatly appreciated. The authors are also grateful to Dr. Robert Williams of NIST for his cooperation, support, and many valuable discussions during the course of this work.

References:

1. D.I. Poston and H.R. Trellue, Monteburns, Version 2.0, Los Alamos National Laboratory, updated Dec. 2, 2002.
2. H.R. Trellue, private communication, July 2004.
3. Monte Carlo Team, "MCNP – A General Monte Carlo N-Particle Transport Code, Version 5", LA-UR-03-1987, Los Alamos National Laboratory, April 24, 2003.
4. S. Ludwig, "Revision to ORIGEN2 – Version 2.2," Oak Ridge National Laboratory, May 23, 2002.
5. L. Cheng, A. Hanson, D. Diamond, J. Xu, J. Carew, and D. Rorer, "Physics and Safety Analysis for the NIST Research Reactor", BNL-NIST-0803, Rev. 1, Brookhaven National Laboratory, April 2004.
6. A.L. Hanson and D.J. Diamond, "Neutronic Analysis of a Proposed Fuel Management Scheme for the NBSR", memo to file dated December 21, 2004.
7. A.L. Hanson and D.J. Diamond, "Neutronic Analysis of a Proposed Fuel Management Scheme for the NBSR with Shim Arm #3 Withdrawn", memo to file dated December 21, 2004.
8. John R. Lamarsh, Introduction to Nuclear Reactor Theory, Addison-Wesley Publishing Company, Inc. Reading, Mass, 1966, p.477.
9. R. Williams, private communication.
10. D.I. Poston and H.R. Trellue, "User's Manual, Version 2.0 for Monteburns, Version 1.0", LA-UR-99-4999, Los Alamos National Laboratory, September 1, 1999.
11. J.F. Briesmeister, Ed., "MCNP – A General Monte Carlo N-Particle Transport Code, Version 4B", LA-12625-M, Version 4B, Los Alamos National Laboratory, March 1997.
12. S. Ludwig, "ORIGEN2, Version 2.1 Release Notes," Oak Ridge National Laboratory, August 1, 1991.

Table 1. Critical Angles for Six Inventories

Time step	Angle from Vertical	k_{eff} (from MCNP)
Startup Core	-19.3°	1.00101 ± 0.00029
1 day Equilibrium Core	-14.6°	1.00006 ± 0.00028
¼ cycle	-11.5°	1.00502 ± 0.00028
Mid cycle	-9.0°	1.00311 ± 0.00027
¾ cycle	-5.0°	1.00393 ± 0.00027
End of Cycle	0°	1.00125 ± 0.00027

Table 2. The % Difference Between the Power in the Upper and Lower Fuel Element Halves as Determined from the Axial Power Peaking

Fuel Element Position	Fuel Management Designation	PD in Lower Core [5]	PD in Lower Core*
A-4	7-1W	1.33	1.26
C-4	8-6W	1.29	1.16
D-1	8-1W	1.15	1.05
E-2	7-5W	1.37	1.23
F-1	7-2W	1.27	1.14
F-7	8-5W	1.13	1.12
H-1	7-2E	1.32	1.21
J-1	8-1E	1.21	1.13

[5] Analysis from Reference 5
* Present Analysis

COLD SOURCE

			D1		F1		H1		J1			
		C2		E2		<>		I2		K2		
	B3		<>		F3		H3		<>		L3	
A4		C4		E4		<>		I4		K4		M4
	B5		<>		F5		H5		<>		L5	
		C6		E6		<RR>		I6		K6		
			D7		F7		H7		J7			

Figure 1. NBSR Fuel Element Position Designation

COLD SOURCE

			8-1W		7-2W		7-2E		8-1E			
		8-3W		7-5W		<>		7-5E		8-3E		
	7-3W		<>		8-7W		8-7E		<>		7-3E	
7-1W		8-6W		7-7W		<>		7-7E		8-6E		7-1E
	8-4W		<>		8-8W		8-8E		<>		8-4E	
		7-4W		7-6W		<RR>		7-6E		7-4E		
			8-2W		8-5W		8-5E		8-2E			

Figure 2. NBSR Fuel Management Scheme

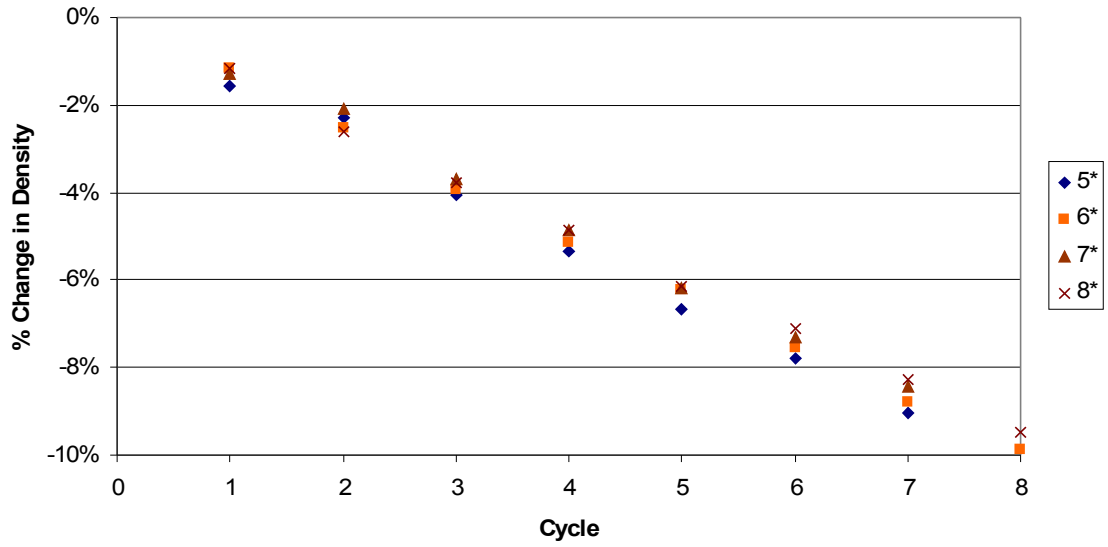

Figure 3. Change in Fuel Density as a Function of Completed Cycle.

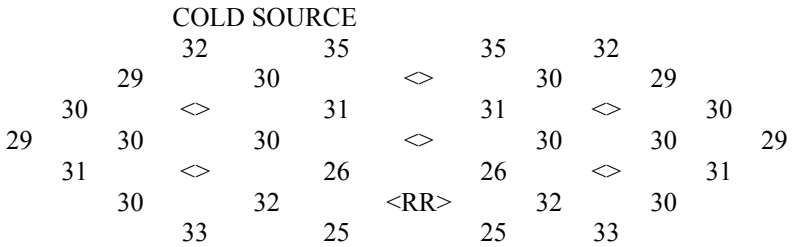

Figure 4. Grams of ^{235}U Burned per Fuel Element, from the Reference Document

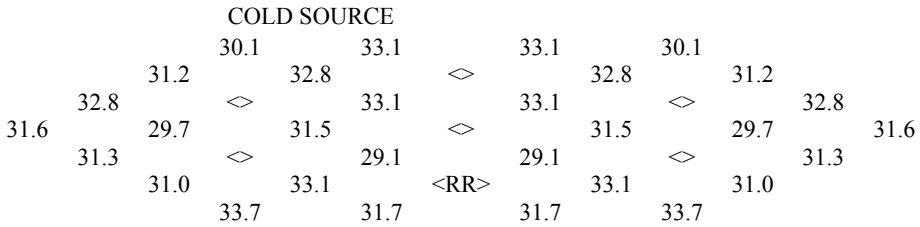

Figure 5. Grams of ^{235}U Burned: Split Core Model:
Upper and Lower Cores Combined

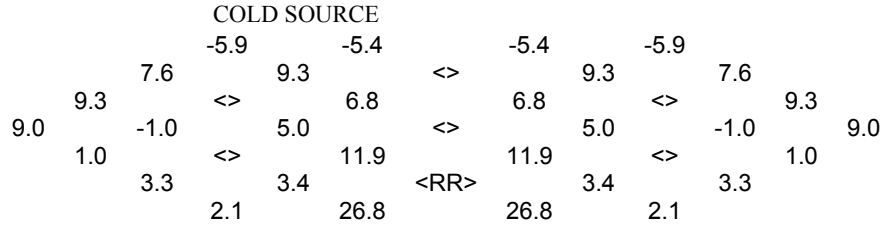

Figure 6. Difference the Between Reference Document and the Present Analysis for the Grams of ^{235}U Burned During Each Cycle in Each Fuel Element (%).

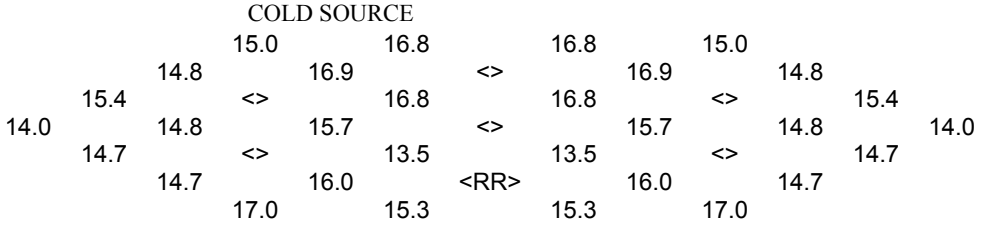

Figure 7. Grams of ^{235}U Burned: Split Core Model: Upper Core

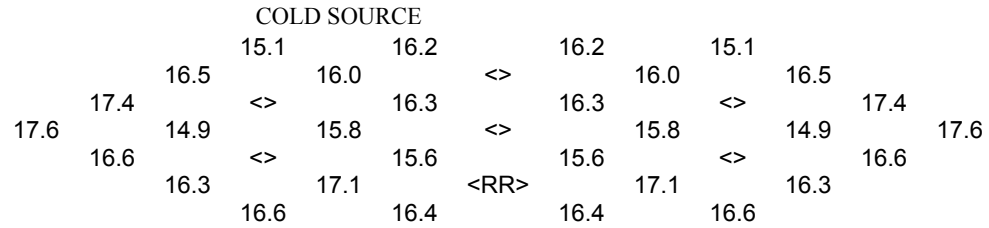

Figure 8. Grams of ^{235}U Burned : Split Core Model: Lower Core

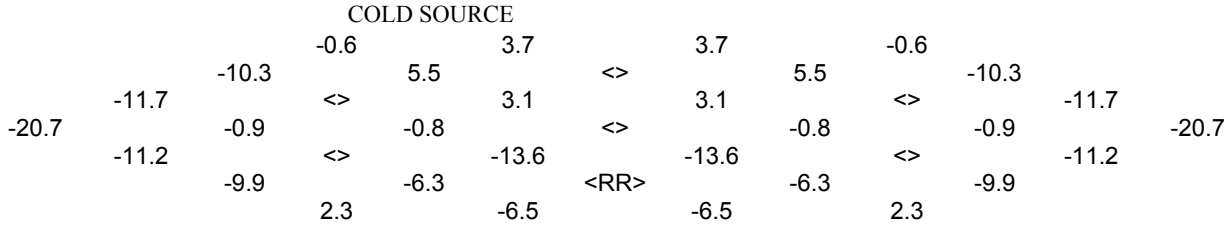

Figure 9. Percent Difference in the ^{235}U Burned Between the Upper and Lower Cores.

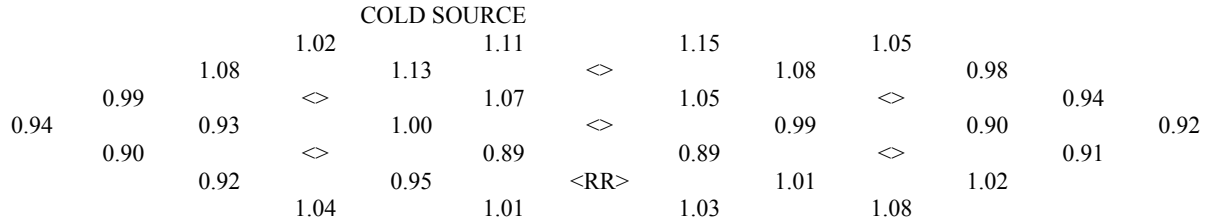

Figure 10. Power Distribution in the SU Core from [5].

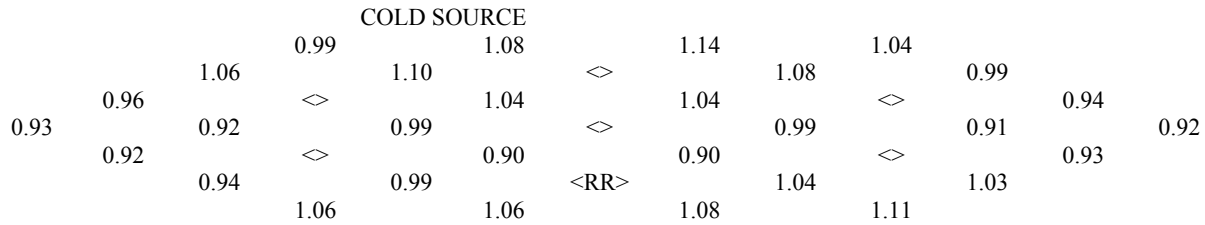

Figure 11. Power Distribution in the SU Core averaged over the upper and lower halves.

COLD SOURCE

			-3.43		-2.70		-1.30		-0.95			
		-2.31		-2.65		<>		-0.46		1.02		
	-3.54		<>		-2.80		-0.95		<>		0.00	
-1.06		-1.08		-1.00		<>		0.00		1.11		-0.54
	2.22		<>		0.56		1.12		<>		1.65	
		1.63		3.68		<RR>		2.48		0.49		
			1.92		4.46		4.37		2.78			

Figure 12. Percent Change from Figure 10 to Figure 11.

COLD SOURCE

			0.90		0.99		1.05		0.98			
		1.02		1.05		<>		1.07		1.08		
	1.07		<>		1.03		1.04		<>		1.11	
1.10		1.00		1.02		<>		1.02		1.00		1.10
	1.03		<>		0.89		0.89		<>		0.99	
		0.99		0.94		<RR>		0.93		0.97		
			0.96		0.91		0.91		0.96			

Figure 13. Power Distribution in the EOC Core from [5].

COLD SOURCE

			0.91		1.00		1.07		1.01			
		1.03		1.04		<>		1.07		1.09		
	1.04		<>		0.99		1.00		<>		1.09	
1.06		0.98		0.98		<>		0.98		0.97		1.07
	1.04		<>		0.86		0.85		<>		1.00	
		1.01		0.97		<RR>		0.97		0.99		
			1.04		0.98		0.98		1.03			

Figure 14. Power Distribution in the EOC Core averaged over the upper and lower halves.

COLD SOURCE

			1.11		1.01		1.90		3.06			
		0.49		-1.43		<>		-0.47		0.46		
	-3.27		<>		-4.37		-3.85		<>		-1.80	
-4.09		-2.50		-4.41		<>		-4.41		-3.00		-3.18
	0.49		<>		-3.93		-4.49		<>		0.51	
		2.02		3.19		<RR>		3.76		2.06		
			1.11		1.01		1.90		3.06			

Figure 15. Percent Change from Figure 13 to Figure 14.

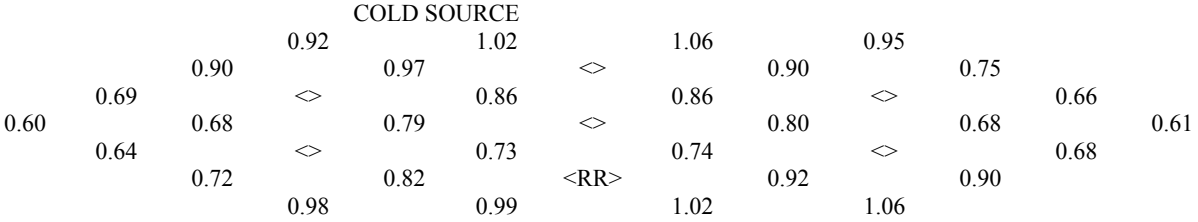

Figure 16. Power Distribution in the Upper Fuel for the SU Core.

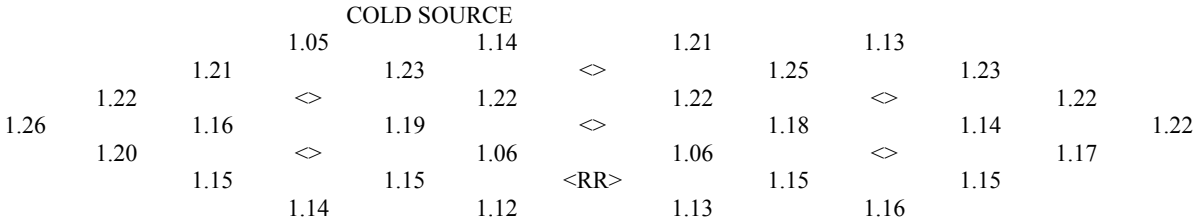

Figure 17. Power Distribution in the Lower Fuel for the SU Core.

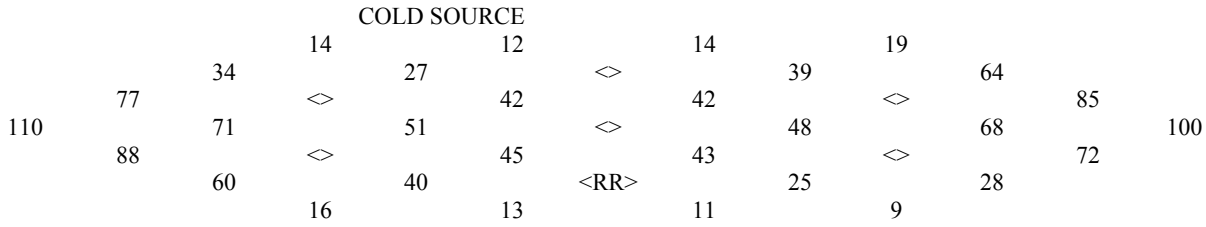

Figure 18. Differences (in%) in the Power Distribution Between the Upper and Lower Cores for the SU Core.

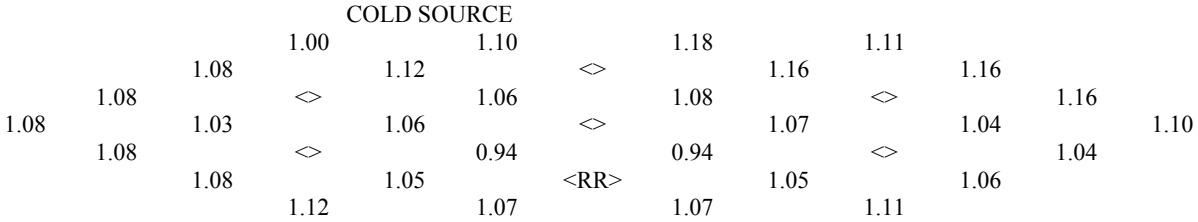

Figure 19. Power Distribution in the Upper Fuel for the EOC Core.

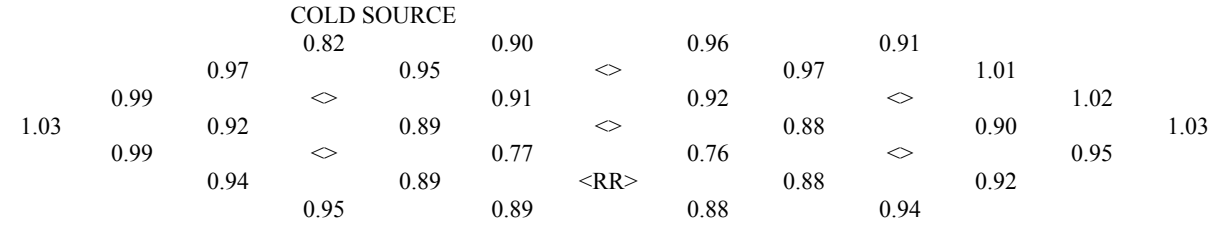

Figure 20. Power Distribution in the Lower Fuel for the EOC Core.

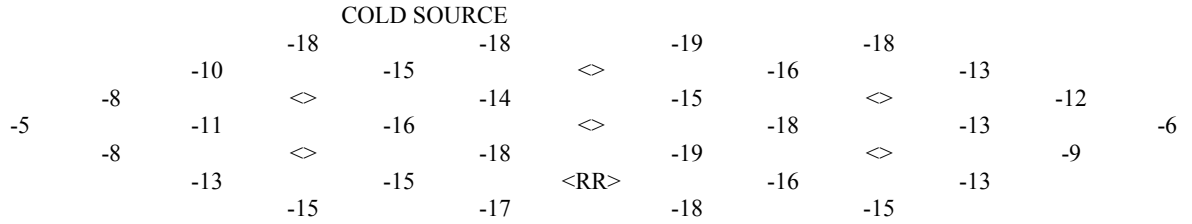

Figure 21. Differences (in%) in the Power Distribution Between the Upper and Lower Cores for the EOC Core.

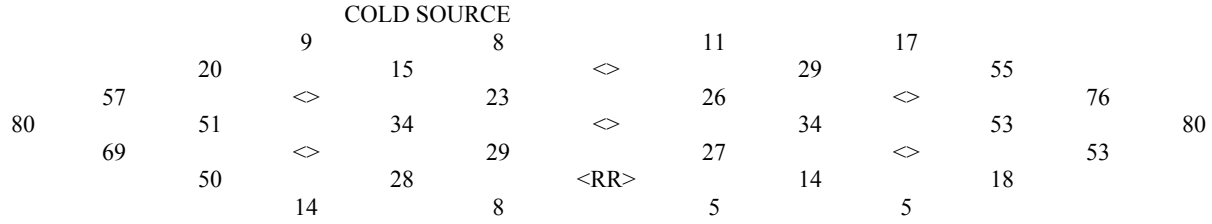

Figure 22. Changes (in %) in the Power Distribution for the Upper Core Between the SU and EOC Cores.

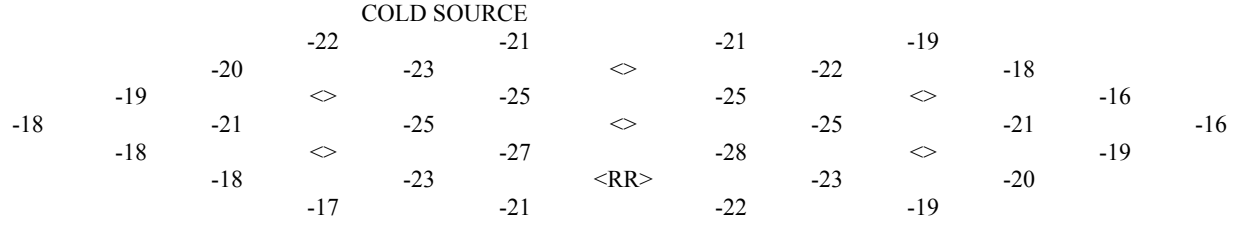

Figure 23. Changes in the Power Distribution for the Lower Core Between the SU and EOC Cores.